REVIEW

Effects of 5f-elements on electronic structures and spectroscopic properties of gold superatom model*

Yang Gao(高阳)[1,2] and Zhigang Wang(王志刚)[1,2,†]

[1] Institute of Atomic and Molecular Physics, Jilin University, Changchun 130012, China

[2] Jilin Provincial Key Laboratory of Applied Atomic and Molecular Spectroscopy (Jilin University), Changchun 130012, China

(Received 20 January 2016; revised manuscript received 9 April 2016; published online 25 June 2016)

5f-elements encaged in a gold superatomic cluster are capable of giving rise to unique optical properties due to their hyperactive valence electrons and great radial components of 5f/6d orbitals. Herein, we review our first-principles studies on electronic structures and spectroscopic properties of a series of actinide-embedded gold superatomic clusters with different dimensions. The three-dimensional (3D) and two-dimensional (2D) superatom clusters possess the 18-electron configuration of $1S^2 1P^6 1D^{10}$ and 10-electron configuration of $1S^2 1P^4 1D^4$, respectively. Importantly, their electronic absorption spectra can also be effectively explained by the superatom orbitals. Specifically, the charge transfer (CT) transitions involved in surface-enhance Raman spectroscopy (SERS) spectra for 3D and 2D structures are both from the filled 1D orbitals, providing the enhancement factors of the order of $\sim 10^4$ at 488 nm and $\sim 10^5$ at 456 nm, respectively. This work implies that the superatomic orbital transitions involved in 5f-elements can not only lead to a remarkable spectroscopic performance, but also a new direction for optical design in the future.

Keywords: 5f-electrons, ds-electrons, superatom, first-principles

PACS: 31.70.–f, 32.30.–r, 36.40.–c, 71.15.Rf **DOI:** 10.1088/1674-1056/25/8/083102

1. Introduction

Gold nanoparticles exhibit strong d–s hybridization and relativistic effects which results in a wide variety of optical phenomena. These properties have attracted a huge interest in the optical studies of bimetallic nanoparticles.[1–4] On the other hand, the spectroscopic properties of actinide also play a remarkable role in the regular arrays of metals.[5–10] The absorption and/or emission lines of 5f valence shell electrons are narrow and sharp in the visible range,[10–12] and these spectra lines could be hardly influenced by the external coordination environment.[5,9] Consequently, the superatom model comprised of f-block and ds-block elements could be envisioned to very likely carry a revolutionary spectroscopic performance.

One of the first superatomic experiments was the seminal work of Knight *et al.* in 1984.[13] They observed conspicuous peaks in the mass spectra of Na clusters containing 2, 8, 20, 40, ... atoms. The electrons in Na [$3s^1$] clusters are confined in quantized orbitals $1S^2$, $1S^2$ $1P^6$, $1S^2$ $1P^6$ $1D^{10}$ $2S^2$ $1S^2$ $1P^6$ $1D^{10}$ $2S^2$ $1F^{14}$ $2P^6$, ..., respectively, and successive electronic shell closure accounts for the enhanced stability of the magic clusters. Subsequent mass spectra of other simple homo- as well as heteroatomic metal clusters have confirmed the relationship between electronic shell closure and enhanced stability.[14] Currently, the electronic structures and derived properties of stable bimetallic gold-based clusters can also be modeled via the superatom models.[14–18] The first predicted superatomic cluster was the icosahedral $W@Au_{12}$ based on density functional theory (DFT) involving the 18-electron count ($1S^2 1P^6 1D^{10}$),[19] which was later confirmed via photoelectron spectroscopy (PES).[20] Soon after that, a series of bimetallic gold superatom models ($M@Au_n$), where M is a d-block atom, have been proposed theoretically.[21–25] Among them, these superatomic clusters all possess a great advantage compared with the pure gold clusters in tuning the excitation light,[26–36] which has been identified on the experimental study.[37–40] Besides, also such as one- and two-photon optical absorption,[41,42] circular dichroism,[43–45] electron paramagnetic resonance spectra,[46] etc. All these optical phenomena can be effectively explained by superatom models.

As is well known the f-block elements have a high density of electronic states, because of their hyperactive valence electrons. This particular attribute has led to an intense interest in optics and magnetic fields in applications of f-element-embedded gold clusters, such as $Ac@Au_7$,[7] $Sg@Au_{12}$,[47] $An@Au_{14}$ (An = Ac, Th, Pa, U),[8,48] $Gd@Au_{15}$,[49] etc. Specific optical characteristics of these superatom models were obtained through their structural and compositional modifications.[26–34] The relevant modification produces spectral shifting in a very wide range that is even as important as the morphological modification in one-component nanoparticles.[50] As reflections of electronic structures, spec-

*Project supported by the National Natural Science Foundation of China (Grant No. 11374004), the Science and Technology Development Program of Jilin Province, China (Grant No. 20150519021JH), the Fok Ying Tung Education Foundation, China (Grant No. 142001), and the Support from the High Performance Computing Center (HPCC) of Jilin University, China.

†Corresponding author. E-mail: wangzg@jlu.edu.cn, or wangzg1978@hotmail.com

© 2016 Chinese Physical Society and IOP Publishing Ltd

troscopic studies of actinide–gold systems that focus on molecular excited-state properties promise our further understanding of actinide–gold bonding schemes and 5f-element electronic structures.

Although in the past several decades much effort has been made to produce and model gold-based bimetallic systems, the understanding of their fascinating properties in the combination systems of ds- and f-elements is still in its infancy. In this paper, we give a concise review of our recent first-principles calculations on electronic structures and spectroscopic properties of actinide-embedded gold superatom models and their recent progress. In Section 2, we demonstrated possible methods to deal with heavy metal clusters that contain ds and f-electrons. In Section 3, we analyze the electronic structures and spectroscopic properties of one-dimensional (1D), two-dimensional (2D), three-dimensional (3D) models, and list the specific molecular orbitals (MOs) that are associated with the corresponding absorption spectra. Finally, a brief conclusion and perspectives on these superatom models are presented in Section 4.

2. Methods

There are some theoretical challenges associated with studying heavy metal clusters.[51–54] Firstly, quantum calculation involving a large number of electrons is computationally extremely challenging, in addition, strong relativistic effects must be considered for each heavy atom. In this review, the electronic structures and spectroscopic properties of actinide-embedded gold superatom models were calculated by using DFT and time-dependent DFT (TDDFT) with relativistic effective core potential (RECP) approach,[55–59] respectively. A significant advantage of these methods is that for systems containing heavy metal elements, the electron correlations can be handled effectively without significantly increasing the computational cost.[60–62] Meanwhile, the RECP approach can effectively consider the scalar relativistic effects, which is crucial for describing the behaviors of ds- and f-electrons.[63] Moreover, because the spin–orbit coupling (SOC) effects play an important role in the excited-state calculation of medium-sized gold clusters,[64–67] the SOC effects within the framework of zero-order regular approximation (ZORA) were also considered in the following calculations.

Absolute Raman intensities are presented as the differential Raman scattering cross-section (DRSC). For Stokes scattering with an experimental setup of a 90° scattering angle and perpendicular plane-polarized light, the cross-section is given as[68]

$$I_{\mathrm{Raman}} = \left(\frac{\mathrm{d}\sigma}{\mathrm{d}\Omega}\right)_i = \frac{(2\pi)^4}{45}\frac{h}{8\pi^2 c\omega_i}\frac{(\omega_0-\omega_i)^4}{1-\exp(-hc\omega_i/k_{\mathrm{B}}T)} \times \left[45\left(\frac{\mathrm{d}\sigma}{\mathrm{d}Q_i}\right)^2 + 7\left(\frac{\mathrm{d}\gamma}{\mathrm{d}Q_i}\right)^2\right].$$

Here, ω and ω_i respectively denote the frequencies of the incident light and the i-th vibrational mode $\mathrm{d}\sigma/\mathrm{d}Q_i$ and $\mathrm{d}\gamma/\mathrm{d}Q_i$ respectively refer to the derivatives of the isotropic and anisotropic polarizability of the i-th vibrational mode h is the Planck constant, c is the light speed, k_{B} is the Boltzmann constant, and T is the Kelvin temperature. The finite lifetime is included phenomenologically using a damping parameter $\Gamma \approx 0.004$ a.u. (The unit a.u. is short for atomic unit), which is reasonable for metal clusters and resonant Raman intensities.[69]

3. Electronic structures and spectroscopic properties

3.1. Electronic structures

These superatom models of actinide-embedded gold clusters can be expressed by a formula

$$[X^{(n)}\mathrm{Au}_m]^q,$$

where X represents an f-block atom, n denotes the number of valence electrons of X atom, m is the size of gold clusters (on the assumption that the gold atom has only one (6s) valence electron), and the superatom may have an overall charge q. All the shell closings (hence the electronic stability) can be evaluated with an "effective gold valence" from

$$N = n + m - q.$$

If N corresponds to a magic number (2, 8, 18, 34, 58, etc.) commonly linked with electronic stability, the superatom complex may be particularly stable. When N is not equal to one of these magic numbers, the complex is expected to have a different structure instead of a spherical one.[65]

3.1.1. Actinium, thorium protactinium or uranium embedded into Au_{14} cage

Currently, doped gold clusters have become a subject of high interest research because of their stable physicochemical activities and unique geometric structures.[70,71] The interactions between the encapsulated atoms and gold clusters allow fine tuning the formations of nanoparticles agglomerates, resulting in more compact structures with lower energy.[72–74] Among them the endohedral gold clusters encapsulating a foreign atom (such as $\mathrm{W@Au}_{12}$) have been formed under specific experimental conditions,[19] and the theoretically calculated value (2.02 eV) of electron affinity (EA) is in good agreement with the experimental data (2.08 ± 0.02 eV). Thus, in order to facilitate future experimental validation, we also calculated the EA values of $\mathrm{Th@Au}_{14}$ and $\mathrm{U@Au}_{14}$ clusters. These EA values are at least 2.35 eV, which is higher than 2.02 eV, suggesting a thermodynamically more stable state of $\mathrm{Th@Au}_{14}$ than that of $\mathrm{W@Au}_{12}$.

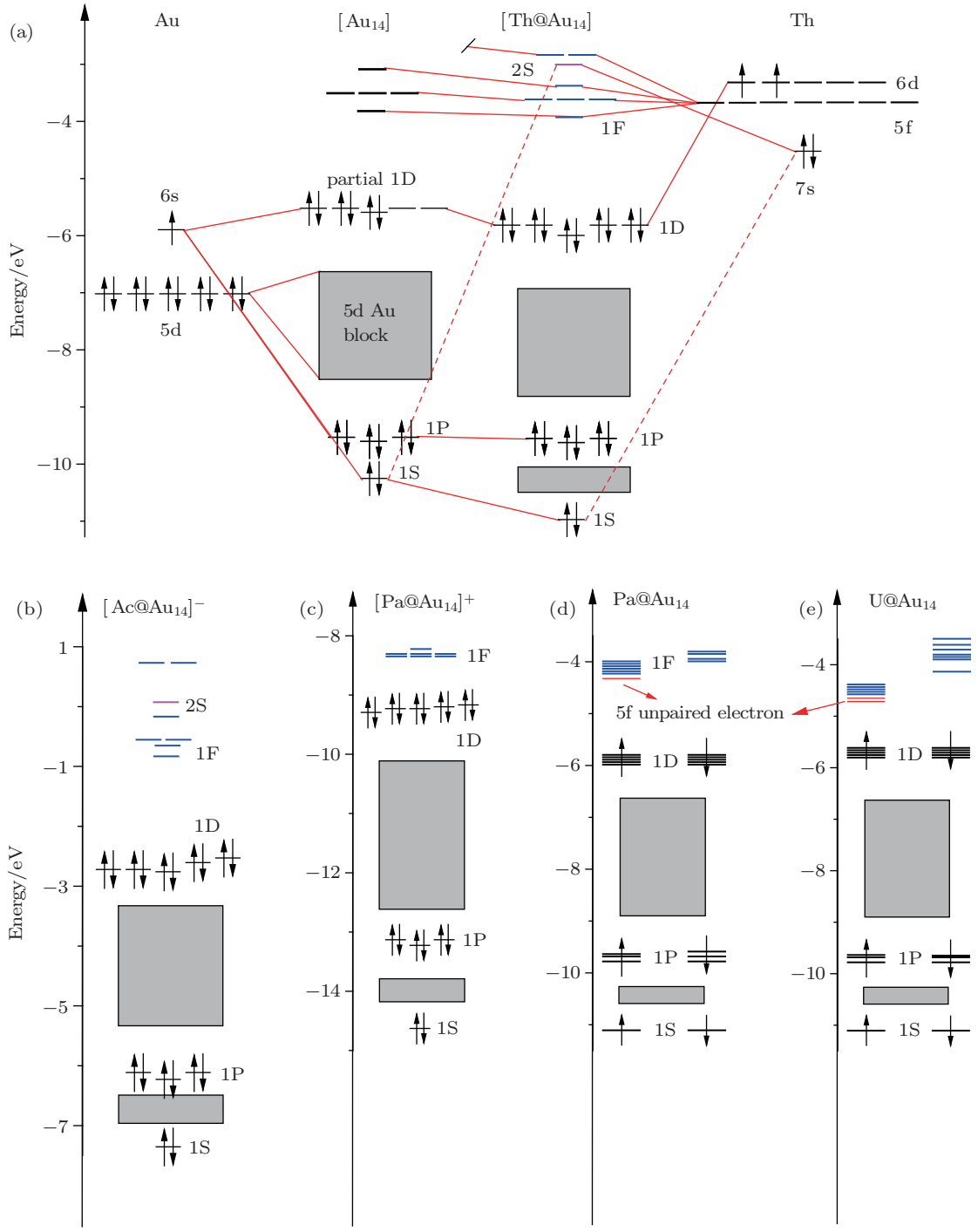


Fig. 1. (color online) MO energy diagrams of the ground state of (a) $Th@Au_{14}$, (b) $[Ac@Au_{14}]^{\cdot-}$, (c) $[Pa@Au_{14}]^{+}$, (d) $Pa@Au_{14}$, (e) $U@Au_{14}$. In panel (a), solid red lines denote the major contributions to the respective MOs, while dashed red lines represent the minor contributions. In panels (d) and (e), the red transverse lines represent occupied molecular orbitals. Upper-case and lower-case letters represent the superatomic and atomic orbitals, respectively. Adapted with permission from Ref. [8]. Copyright 2016 Springer.

In order to understand the electronic structure requirements of actinide-embedded gold superatom models the MO energy diagrams of the ground states of $Th@Au_{14}$, $[Ac@Au_{14}]^{-}$, $[Pa@Au_{14}]^{+}$, $Pa@Au_{14}$, $U@Au_{14}$ are shown in Fig. 1. Considering the similarity in five structures, we will only take the neutral $Th@Au_{14}$ to analyze the electronic and optical properties in detail. It is well known that the electron configurations of isolated Ac, Th, Pa, and U atom are $6d^17s^2$, $6d^27s^2$, $5f^26d^17s^2$, and $5f^36d^17s^2$ which possess a doublet triplet, quartet, and quintet ground state, respectively.[75] However, when interacting with the gold cage in confined systems, the contributions of bonding MOs of these earlier actinide atoms (Ac or Th) are less from 5f shell, and will instead be dominated by 6d and 7s shells. Sometimes, the 7p orbitals will also play a prominent role in the bond formation. In detail taking $Th@Au_{14}$ clusters as a typical example it may be described as $Th^{4+}@[Au_{14}]^{4-}$ with the central Th^{4+} ion and the $[Au_{14}]^{4-}$ cage by a concise and widely used expression. Its electronic

structure satisfies the closed-shell superatomic electron count of 14(Au) + 4(Th) = 18 of the jellium model. Here we assume that the gold atom has only one (6s) valence electron available for bonding in the jellium model. This superatom formulation is similar to those in a series of gold clusters such as W@Au_{12} (W: $5d^46s^2$) and Zr@Au_{14} (Zr: $4d^25s^2$).

As is well known the inherent relativistic effects of the gold clusters can cause apparent hybridization between the inner-shell d orbitals and the outer-shell s orbitals (these hybrid orbitals are named 5d6s orbitals). When foreign atoms are embedded, hybridization becomes more apparent between 5d6s orbitals and the valence electron orbitals of the doped atoms.[19,54] So the formation of Th@Au_{14} cluster (Th: $6d^27s^2$) mainly involves the interaction between the hybrid atomic orbitals of Th and the gold cage orbitals of the polyhedron, namely 1S-Au_{14} (with 2 electrons), 1P-Au_{14} (with 6 electrons), 1D-Au_{14} (with 6 electrons) (see Fig. 1(a)). The spatial shapes of Th@Au_{14} superatomic MOs are shown in Fig. 2. Among them, the occupied bonding 1S-Th@Au_{14} and the unoccupied antibonding 2S-Th@Au_{14} superatomic shell orbitals originate from the combination of 1S-Au_{14} and 7s-Th. The unoccupied 2S shell contains a small contribution from the combination of 6s and 6p atomic orbitals in Au_{14} cage. This phenomenon is similar to the observed hybridization between s and p atomic orbitals in the previously reported $[Sn@Cu_{12}@Sn_{20}]^{12-}$ cluster (with Cu 4p contribution to the superatomic orbitals).[67] Next, the 6d-Th atomic orbitals interact with the 1D-Au_{14} superatomic orbitals to form five 1D-Th@Au_{14} superatomic orbitals. The 7p-Th almost has no interaction with 1P-Au_{14}, because it is located at high-lying level. Therefore, according to the energetic sequence and the nodal shape of the MOs, we can identify a series of superatomic orbitals in the sequence 1S, 1P, 1D corresponding to the 9 lowest-lying filled MOs with 18 electrons, and 1F and 2S corresponding to the 8 virtual MOs (see Fig. 2). In other words, the formation of Th@Au_{14} involves primarily the interaction between the s- and d-type shells of the endohedral atom and the superatomic orbitals of Au_{14} cage.

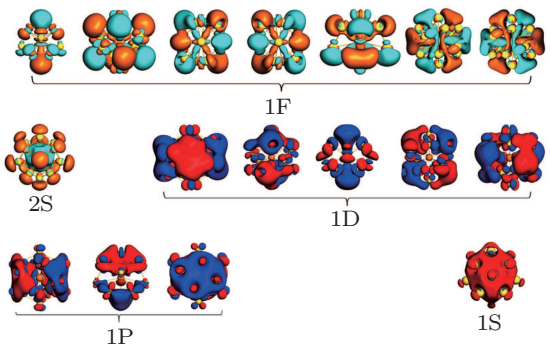


Fig. 2. (color online) Superatomic jelliumatic MOs of the ground state of Th@Au_{14} (isodensity = 0.02 a.u.). Adapted with permission from Ref. [8]. Copyright 2016 Springer.

In addition, we also compare the electronic structures of the isoelectronic clusters $[Ac@Au_{14}]^-$ and $[Pa@Au_{14}]^+$ (Ac: $6d^17s^2$; Pa:$5f^26d^17s^2$), which all satisfy the 18-electron configuration of $1S^21P^61D^{10}$ jellium state (see Figs. 1(b) and 1(c)). For the neutral Pa@Au_{14} and U@Au_{14} clusters, our analysis shows that they are magnetic and have one and two 5f-unpaired electrons in addition to the 18-electron jellium state, respectively. Our analysis also indicates that the spin contributions of the Pa atom and U atom are 0.76 e and 2.03 e, respectively (see Figs. 1(d) and 1(e)). In the two neutral clusters, the 5f shell electrons account for > 85% of the contributions to the single-electron-occupied orbitals. On the other hand, for the two-electron occupied orbitals, their spatial shapes reflect their "covalent bonds" between the Pa/U atom and Au_{14}-cage, i.e., superatomic 1D orbitals. Other superatomic orbitals (1S, 1P) have also been found at low-lying levels.

It should be noted that for highly symmetric clusters, Jahn–Teller (JT) distortions become operative in some cases because of the interelectronic repulsion caused by vibronic interactions.[76,77] (e.g., splitting of t_{2u} orbitals via JT distortion under O_h symmetry). As a result, the optimized D_{2d} structure of $[Ac@Au_{14}]^-$ is very similar to that of Th@Au_{14}, the $[Pa@Au_{14}]^+$, Pa@Au_{14}, and U@Au_{14} analog instead adopt a C_1 symmetry. This difference can be attributed to the sizes of the four actinide metal atoms: namely, Ac, 1.86; Th, 1.75; Pa, 1.69 Å, and U, 1.70 Å.[78] In the Th@$Au_{14}D_{2d}$ cluster, inclusion of the SOC effects causes the Th–Au bond length to be shortened by ~ 0.2 Å in comparison with that obtained by including the scalar relativistic effects. Furthermore, the HOMO–LUMO (highest occupied molecular orbital–lowest unoccupied molecular orbital) gap value also decreases from 1.92 eV to 1.82 eV (see Fig. 3).

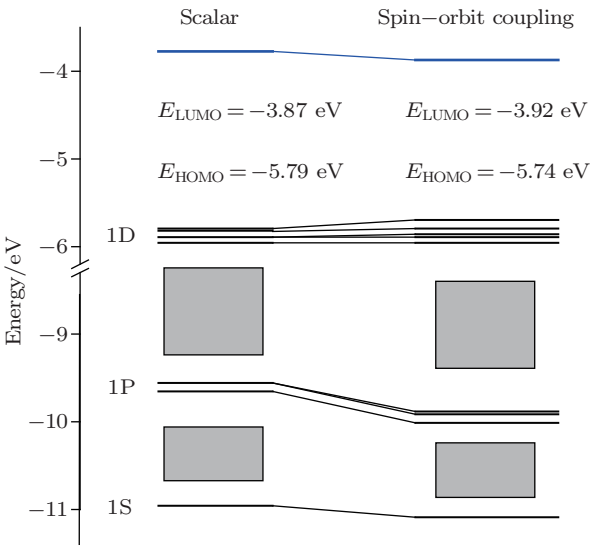


Fig. 3. MO diagrams for the Th@Au_{14} cluster including relativistic effects with (right) and without (left) spin–orbit couplings. Adapted with permission from Ref. [8]. Copyright 2016 Springer.

3.1.2. Actinium- or lanthanum-embedded into Au_7 planar structure

In fact, the superatom models are also generalized to the 2D planar structures.[73,79] The preference of planar structure

is attributed to the relativistic effects that cause the size of the 6s orbitals to shrink and thus enhances the s–d hybridization. Taking the Ac@Au_7 cluster as a framework, the Au_7-D_{7h} ring has a nearly cylindrical symmetry (see Fig. 4(a)). Since each gold atom possesses one valence 6s electron, the total number of the itinerant electrons is 7 and hence the electron configuration of this cluster is $1S^2 1P_x^2 1P_y^2 1D_{xy}^1$, while the in-plane other 1D and all 1F orbitals are unoccupied. The in-plane D_{xy} and $D_{x^2-y^2}$ orbitals are more stable than the D_{xz}, D_{yz}, and D_{z^2} orbitals which is analogous to a crystal field splitting. For the isolated Ac atom, it can be viewed as a $6d^3$ electron configuration, because its two 7s electrons easily enter into the 6d shell. Thus, in the case of Ac-doped clusters, the number of delocalized electrons for Ac@Au_7 adds up to 10 that represents a closed-shell electronic structure with a $1S^2 1P^4 1D^4$ electron structure (see Fig. 4(a)). Due to the fact that the s–p overlap is maximized when both Au and Ac atoms are in the same plane (or on the same line), these superatom orbitals are enough to enhance the planarity of such small clusters. A physically similar effect was found in Ti@Au_6 and Sc@Cu_7[80–82] clusters, which were responsible for the planarity. On the other hand La@Au_7.[83] also possesses the 10-electron configuration of $1S^2 1P^4 1D^4$ because of La atom with $5d^1 6s^2$ configuration (see Fig. 4(b)).

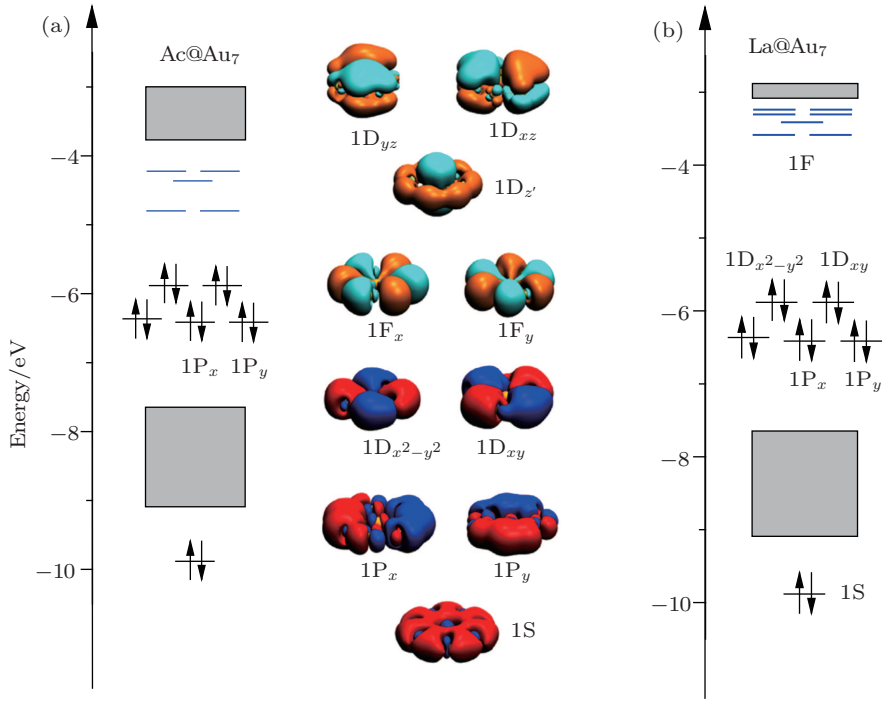


Fig. 4. (color online) MO energy diagrams of the ground state of (a) Ac@Au_7 and (b) La@Au_7, and the superatomic jelliumatic MOs of Ac@Au_7 cluster.

The average total binding energies of per atom and HOMO–LUMO gap for Ac@Au_7 are 2.70 eV and 2.42 eV respectively, and those for La@Au_7 are 2.79 eV and 2.35 eV respectively. In general, nanocluster structures with binding energy greater than 2.40 eV and HOMO–LUMO gap larger than 1.70 eV are commonly regarded as being stable.[21] Therefore, our current results suggest that Ac@Au_7 and La@Au_7 both belong to stable structures.

3.1.3. Dimer of actinium and gold atoms

For the 1D diatomic clusters, our previous work[33,34] based on DFT calculations has pointed out that the presence of the heteronuclear metal atoms can modify the electronic structures and electronic absorption spectra of binary coinage metal clusters. The binary coinage metal clusters also have great advantages in tuning the excitation light for SERS spectra compared with the pure element clusters. Thus, in order to explore the role of 5f-element in the actinide–gold dimer, we studied the Ac–Au molecule.

The actinium and gold atoms have the valence electronic configurations of $6d^1 7s^2$ and $5d^{10} 6s^1$ respectively. The lowest energy state of AcAu dimer is predicted to be singlet (see Fig. 5). In general, for the unsaturated $6s^1$ and $6d^1$ shell one would expect this state to be able to form a sigma (6s–6d) chemical bond. But, the analyses of MOs show that the 7p orbital also plays an important role through 7s7p hybridization in bonding. Exemplifying the 11σ (HOMO) and 10σ (HOMO-1), the former is formed by the hybridization of $6d_z^2$, 7s, and $7p_z$ orbitals with only little antibonding character, while the latter is formed by the bonding interaction largely between the 6s-Au and 7s-Ac, and contains little 7s-Ac and $7p_z$-Ac components. The compositions of $3\delta_{x^2-y^2}$ and $3\delta_{xy}$ MOs all come from the atomic orbitals of the gold atom, and the $6\pi_x$ ($6\pi_y$) MO corresponds to the hybridization between $5d_{xz}$ ($5d_{yz}$) of the gold atom and $6d_{xz}$ ($6d_{yz}$) of the actinium atom. The MO ($3\delta_{x^2-y^2}$) and MO ($3\delta_{xy}$), and MO ($6\pi_x$) and MO ($6\pi_y$) are double-degenerate orbitals. Moreover, the 9σ MO is largely

dominated by the $5d_z^2$ and $6d_z^2$, presenting a bonding interaction.

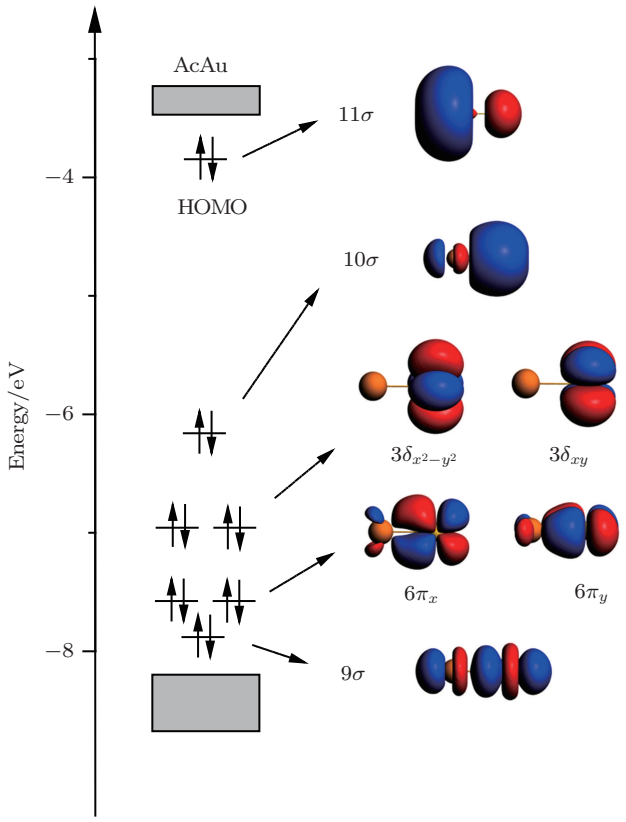


Fig. 5. (color online) Energy diagrams and MO shapes of the ground state of AcAu dimer.

3.2. Spectroscopic properties

3.2.1. 3D Th@Au_{14} cage-cluster

For the particular clusters, the electronic absorption spectrum is often used to identify the validity of the superatom model, because the allowed transitions involve mainly the superatomic (jelliumatic) orbitals in a low-energy range.[65,84,85] Thus, based on the above discussion on the electronic structures of actinide-embedded gold superatom models, we further analyzed the absorption spectra of pyridine-Th@Au_{14} complexes as shown in Fig. 6. In fact, for the bare metal clusters, the absorption spectrum is mainly due to intracluster excitation. However, when pyridine molecule is adsorbed on its surface, in addition to intracluster transition contribution, the interaction between pyridine molecule and metal cluster can also result in a new charge-transfer (CT) excitation transition from the metal to the molecule. The CT resonant phenomenon is very sensitive, when the incident light is resonant with a molecular or CT excitation of the system,[69,86–88] so it is difficult to control and obtain experimentally.

In order to thoroughly understand the interaction between the molecule and the metal, we first listed the well-known six vibrational modes and corresponding frequencies of the pyridine molecule, namely, ring deformation modes (~ 598 cm^{-1}), ring breathing modes (~ 978 cm^{-1} and ~ 1021 cm^{-1}) and ring stretch vibrational modes (~ 1205 cm^{-1}, ~ 1468 cm^{-1}, $\sim 1568/1574$ cm^{-1}), which all have exhibited very strong signals in SERS experiment.[89,90] The static Raman scattering spectrum of pyridine is mainly dominated by ring breathing and ring stretch modes. The relative Raman intensities of these vibrational modes are closely related to the adsorption site of pyridine molecule. For the three pyridine-Th@Au_{14} complexes (gold atoms possess three kinds of coordination types, see the inset in Fig. 6), the maximum static Raman peak corresponds to ring breathing vibrational mode (~ 954 cm^{-1}), and its intensity enhances about 4 $\sim$ 14 times compared with that of pyridine alone. Besides, the typical static Raman peaks also show a blue shift of about 1 cm^{-1} $\sim$ 35 cm^{-1}, which is consistent with the previous theoretical calculation for a pyridine molecule adsorbed on Ag_{20} surface.[69] All these changes are induced by the polarization effect caused by charge redistribution of complex.

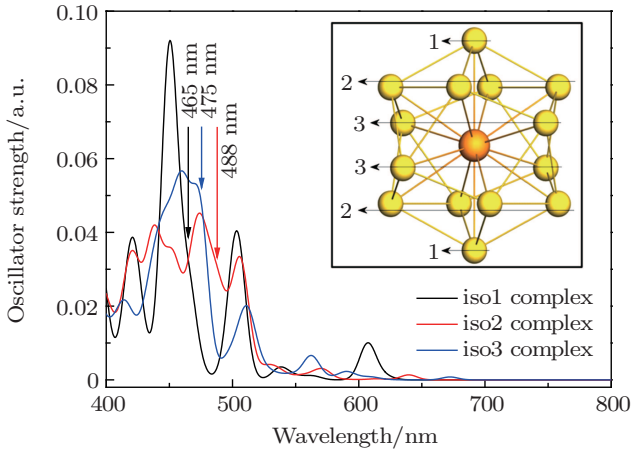


Fig. 6. (color online) Absorption spectra of the pyridine-Th@Au_{14} complex at three different adsorption sites. The three different colored lines (1, 2, 3) denote three coordination types of the gold atoms (iso1, iso2, and iso3), serving as prospective adsorption sites for pyridine molecules in unit SERS study. Absorption coefficients are given as the oscillator strength in unit a.u. and wavelength in nm. Spectra were broadened by Lorentzian function with a width of 15 cm^{-1}. Adapted with permission from Ref. [8]. Copyright 2016 Springer.

Next, based on the typical CT resonance excitations, the SERS spectra ranging from 300 cm^{-1} to 1800 cm^{-1} for three typical pyridine-Th@Au_{14} complexes were simulated, as shown in Fig. 7. The typical absorption peaks are located at 465 nm, 488 nm, and 475 nm, respectively (see Fig. 6).[8] These excitation lines correspond to the Raman scattering intensities and are 10^{-28} cm^2/sr, 10^{-28} cm^2/sr, and 10^{-27} cm^2/sr, representing enhancements of 10^3, 10^3, and 10^4 compared with the static Raman scattering intensity of pyridine molecule (10^{-31} cm^2/sr). Importantly, for the previously reported absorption spectrum originating from a pyridine molecule adsorbed on pure gold clusters, the CT excitations are almost completely concealed by metal–metal transitions.[91] Thus, the study suggests a novel enhancement mechanism which can exist in an actinide-encapsulated gold cluster system, and further improvement in the enhancement magnitude might be expected.

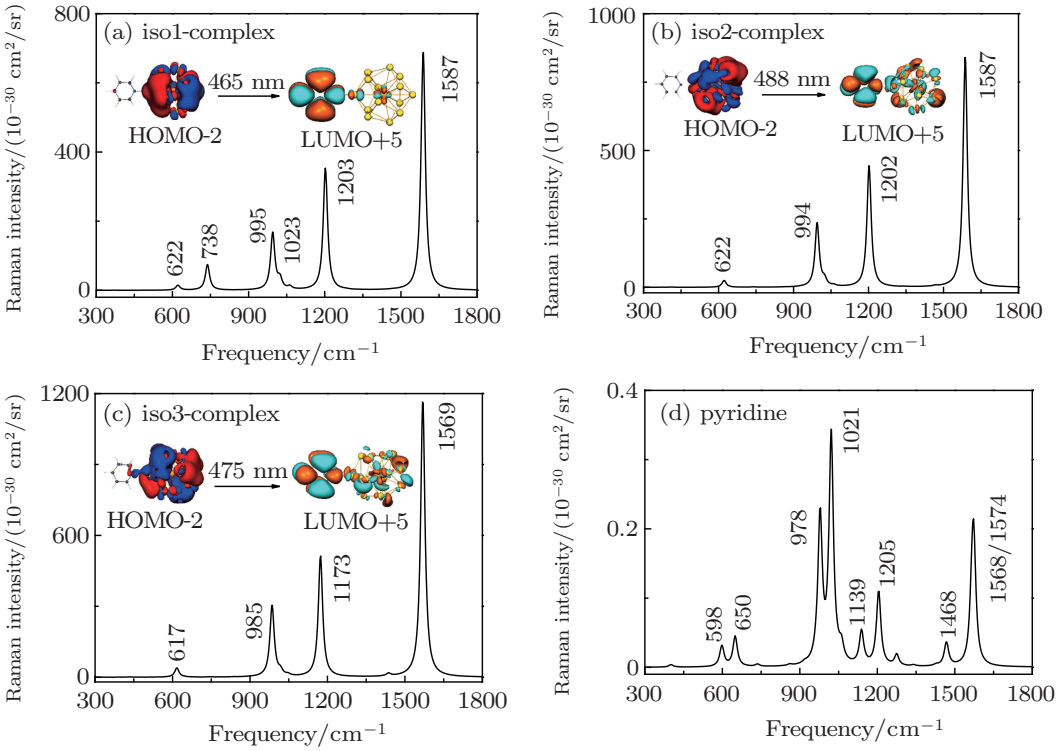


Fig. 7. (color online) Charge-transfer resonance-enhanced Raman spectra, calculated at DFT level for three pyridine-Th@Au_{14} complexes at three different adsorption sites, corresponding to iso1 (a), iso2 (b), and iso3 (c) as indicated by the inset in Fig. 6. The static Raman spectra for pyridine are given in panel (d). Differential cross-sections are measured in the units of 10^{-30} cm^2/sr, and these spectra are broadened by the Lorentzian function with a width of 20 cm^{-1}. Reproduced with permission from Ref. [8]. Copyright 2016 Springer.

3.2.2. 2D Ac@Au_7 planar-structure

For the two-dimensional P-complex and V-complex, the typical absorption peak of the P-complex is located at 370 nm (see Fig. 8(a)). The Raman scattering intensity is of the order of 10^{-28} cm^2/sr, showing an enhancement of the order of 10^3 in comparison with the 10^{-31} cm^2/sr of pyridine. However, for the V-complex, the typical absorption peak is located at 456 nm (see Fig. 8(a)). The intensity of the order of 10^{-26} cm^2/sr corresponds to an enhancement of the order of 10^5. All the SERS spectra based on typical CT resonance excitations are shown in Fig. 9. Next, we also simulated the CT resonance-enhanced Raman spectra for pyridine-Au@Au_7 complexes under their own corresponding excited lines (see Fig. 8(b)). Among them, although the CT enhances intensities ($\sim 10^4$) for P_2-complex and V_2-complex, they are still lower than that of V-complex, and the four complexes are distorted seriously.[7] Furthermore, the MOs analysis for V-complex shows that the electron transition is from the 1D (6d orbital of Ac, 5d6s hybrid orbital of Au_7 ring) superatomic orbital to the π orbital of pyridine. However, for the other five complexes, the electrons involved in excited transitions are all from 5d or 5d6s hybrid orbitals of Au_7 ring. Therefore, the 6d electron involved in excited transitions is more likely to lead to a strong CT enhancement.

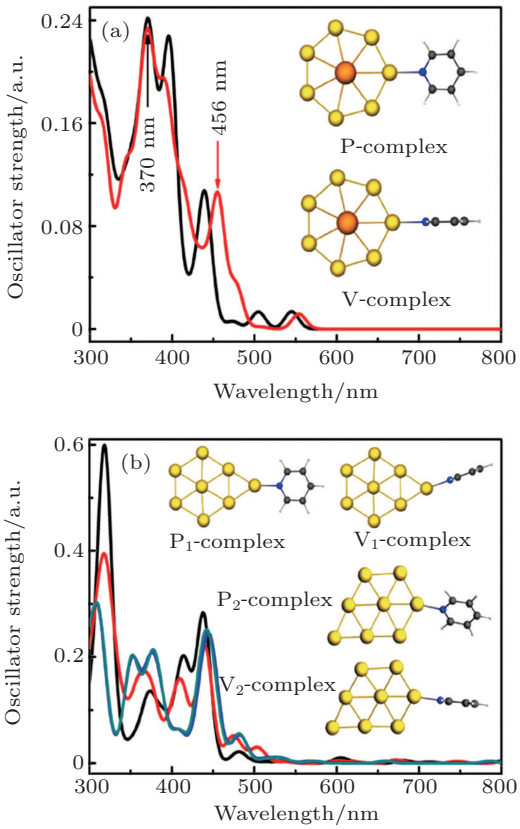


Fig. 8. (color online) Absorption spectra and stable structures of (a) P-complex and V-complex, (b) P_1-complex, V_1-complex. P_2-complex, and V_2-complex, respectively. The subscripts 1 and 2 represent the different adsorption sites of Au_8 structure. (Ac: orange, Au: luminous yellow, N: deep blue, C: deep grey, H: white). Adapted with permission from Ref. [7]. Copyright 2015 Royal Society of Chemistry.

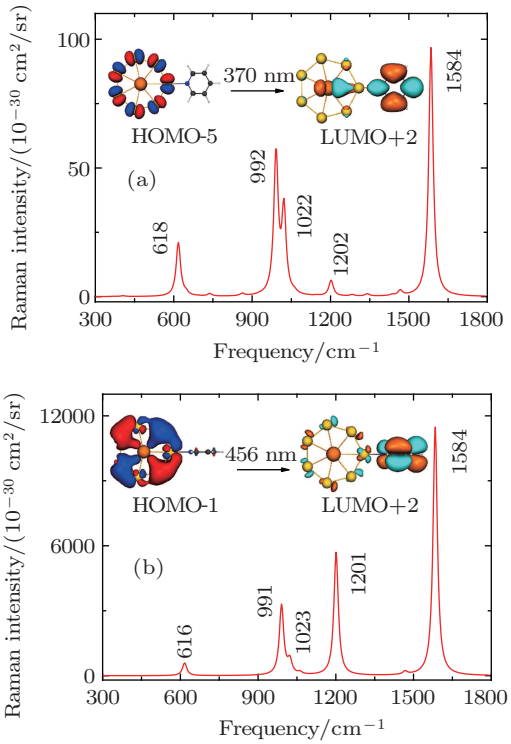


Fig. 9. (color online) Calculated CT resonance-enhanced Raman spectra of (a) P-complex, (b) V-complex at the corresponding incident wavelength. Adapted with permission from Ref. [7]. Copyright 2015 Royal Society of Chemistry.

In short, the optical absorption and SERS spectra of the 2D or 3D structures are strongly dependent on their electronic structures. Near the frontier MOs, each of these systems typically consists of a sparse set of superatomic orbitals, which arise primarily from the Au (6s) or actinide (5f, 6d or 7s) atomic orbitals. Furthermore, these superatomic orbitals can be split into several sets due to the limitation of symmetry. This splitting has an important effect on the optical absorption spectrum as multiple peaks result from transitions between superatomic orbitals. For the 2D or 3D complexes we studied, their electronic transitions are all from filled 1D superatom orbitals to virtual π bonding orbital of the pyridine ring. Also, all the maximum CT excitation bands are localized in the blue laser band, and commonly used in Raman spectrum measurement, especially the 488 nm, indicating SERS substrate materials containing actinide elements would have great advantages in adjusting excitation light.

4. Conclusions and perspectives

We have designed a superatomic model series with different dimensions via first-principles DFT calculations. The 3D nanocage structures $[An@Au_{14}]^n$ (where An = Ac, Th, Pa or U; $n = -1$, 0 or $+1$, respectively), all satisfy the 18-electron configuration of $1S^2 1P^6 1D^{10}$ jellium state that is analogous to the previously reported electronic structures such as $W@Au_{12}$,[19] wherein the bonding involves primarily interactions between the s- and d-type shells of the endohedral atom and those of the gold-cage superatom (Au 6s orbitals). However, for the magnetic clusters ($Pa@Au_{14}$ and $U@Au_{14}$), these 5f-electron MOs maintain their original atomic orbital characteristics, and exhibit characteristics similar to those of the endohedral metallofullerenes (EMFs)[92–94] or passivated quantum dots.[95–100] The 2D planar structures, $An@Au_7$ (An = La or Ac), each represent a closed-shell electronic structure with a $1S^2 1P^4 1D^4$ jellium model state, which is similar to previously reported structures, such as $Ti@Au_6$, $Sc@Cu_7$.[80,81] The 1D AcAu dimer structure is mainly formed by the combination of sigma and pi bonding orbitals. Next, a number of spectroscopic properties have been calculated and analyzed by TDDFT method. The results indicate that the allowed optical transitions involve mainly the superatomic orbitals. Furthermore, the CT-SERS spectra involve electronic transitions that are all from the filled 1D orbitals, which reveals the enhancement factors are of the order of $\sim 10^4$ at 488 nm for 3D nanocage structures and of the order of $\sim 10^5$ at 456 nm for 2D planar structures, respectively.

The above research results show that the superatom model formed from the coupling between 5f- and ds-electron can not only extend the wavelength range of electronic absorption spectra, but also bring a novel enhancement mechanism in the practical application, such as SERS spectra,[10,101] etc. So the superatom model containing 5f elements might improve the spectroscopic characteristics dramatically beyond previous implementations based on traditional atom models in the past. However, although the actinide-embedded superatom model has exhibited various advantages in theoretical simulations, the new field still faces multiple challenges including the modification of electronic structures the design of principle, and the condition of artificial synthesis, and so on.

Acknowledgment

We would like to thank Prof. Boon K Teo, Prof. Ruhong Zhou, Dr. Lei Chen, Dr. Bo Wang, Dr. Jun Liu, Dr. Jia Wang, Mr. Wanrun Jiang, Ms. Yanyu Lei, Mr. Dexuan Xu, Mr. Zhiyuan Zhang, Ms. Tianrong Yu for the stimulating discussion.

References

[1] Pyykkö P 2008 *Chem. Soc. Rev.* **37** 1967
[2] Boisselier E and Astruc D 2009 *Chem. Soc. Rev.* **38** 1759
[3] Häkkinen H 2008 *Chem. Soc. Rev.* **37** 1847
[4] Giljohann D A, Seferos D S, Daniel W L, Massich M D, Patel P C and Mirkin C A 2010 *Angew. Chem. Int. Ed.* **49** 3280
[5] Katz J, Seaborg G and Morss L 1986 *The chemistry of the actinide elements*, Volume II (Now York: Methuen, Inc.)
[6] Krupa J 1995 *J. Alloys Compd.* **225** 1
[7] Gao Y, Chen L, Dai X, Song R X, Wang B and Wang Z G 2015 *Rsc. Adv.* **5** 32198
[8] Gao Y, Wang B, Lei Y Y, Teo B K and Wang Z G 2016 *Nano Res.* **9** 622

[9] Da Re R E, Jantunen K C, Golden J T, Kiplinger J L and Morris D E 2005 *J. Am. Chem. Soc.* **127** 682
[10] Ravindran T R and Arora A K 2011 *J. Raman Spectrosc.* **42** 885
[11] Jha A 2014 *Rare Earth Materials: Properties and Applications* (Florida: CRC Press)
[12] Henriksen G, Bruland O S and Larsen R H 2004 *Anticancer Res.* **24** 101
[13] Knight W D, Clemenger K, de Heer W A, Saunders W A, Chou M and Cohen M L 1984 *Phys. Rev. Lett.* **52** 2141
[14] Jena P 2013 *J. Phys. Chem. Lett.* **4** 1432
[15] Reveles J U, Clayborne P A, Reber A C, Khanna S N, Pradhan K, Sen P and Pederson M R 2009 *Nat. Chem.* **1** 310
[16] Teo B K and Zhang H 1995 *Coord. Chem. Rev.* **143** 611
[17] Janssens E, Neukermans S and Lievens P 2004 *Curr. Opin. Solid State Mater. Sci.* **8** 185
[18] Khanna S N and Jena P 1992 *Phys. Rev. Lett.* **71** 208
[19] Pyykkö P and Runeberg N 2002 *Angew. Chem. Int. Ed.* **114** 2278
[20] Li X, Kiran B, Li J, Zhai H J and Wang L S 2002 *Angew. Chem. Int. Ed.* **41** 4786
[21] Gao Y, Bulusu S and Zeng X C 2006 *Chem. Phys. Chem.* **7** 2275
[22] Wang L M, Bulusu S, Zhai H J, Zeng X C and Wang L S 2007 *Angew. Chem. Int. Ed.* **46** 2915
[23] Gao Y, Bulusu S and Zeng X C 2005 *J. Am. Chem. Soc.* **127** 15680
[24] Zhang C H, Cui H and Shen J 2012 *Chin. Phys. B* **21** 103102
[25] Xu H G, Wu M M, Zhang Z G, Sun Q and Zheng W J 2011 *Chin. Phys. B* **20** 043102
[26] Olivares-Amaya R, Rappoport D, Munoz P A, Peng P, Mazur E and Aspuru-Guzik A 2012 *J. Phys. Chem. C* **116** 15568
[27] Patra P P and Kumar G V P 2013 *J. Phys. Chem. Lett.* **4** 1167
[28] Sivanesan A, Witkowska E, Adamkiewicz W, Dziewit L, Kaminska A and Waluk J 2014 *The Analyst* **139** 1037
[29] Suntivich J, Xu Z, Carlton C E, Kim J, Han B, Lee S W, Bonnet N, Marzari N, Allard L F, Gasteiger H A, *et al.* 2013 *J. Am. Chem. Soc.* **135** 7985
[30] Wang Y, Chen L and Liu P 2012 *Chem. Eur. J.* **18** 5935
[31] Yin Y, Qiu T, Ma L, Lang X, Zhang Y, Huang G, Mei Y and Schmidt O G 2012 *J. Phys. Chem. C* **116** 25504
[32] Zhou Y, Lee C, Zhang J and Zhang P 2013 *J. Mater. Chem. C* **1** 3695
[33] Chen L, Li Z, Meng Y, Lu M, Wang Z and Zhang R Q 2013 *J. Phys. Chem. C* **117** 12544
[34] Chen L, Gao Y, Xu H, Wang Z, Li Z and Zhang R Q 2014 *Phys. Chem. Chem. Phys.* **16** 20665
[35] Chen L, Gao Y, Cheng Y, Li H, Wang Z, Li Z and Zhang R Q 2016 *Nanoscale* **8** 4086
[36] Chen L, Gao Y, Cheng Y K, Su Y B, Wang Z G, Li Z Q and Zhang R Q 2015 *J. Phys. Chem. C* **119** 17429
[37] Jensen L, Aikens C M and Schatz G C 2008 *Chem. Soc. Rev.* **37** 1061
[38] Wu D Y, Li J F, Ren B and Tian Z Q 2008 *Chem. Soc. Rev.* **37** 1025
[39] Schlucker S 2014 *Angew. Chem. Int. Ed.* **53** 4756
[40] Valley N, Greeneltch N, Van Duyne R P and Schatz G C 2013 *J. Phys. Chem. Lett.* **4** 2599
[41] Day P N, Nguyen K A and Pachter R 2010 *J. Chem. Theory Comput.* **6** 2809
[42] Ramakrishna G, Varnavski O, Kim J, Lee D and Goodson T 2008 *J. Am. Chem. Soc.* **130** 5032
[43] Yao H, Miki K, Nishida N, Sasaki A and Kimura K 2005 *J. Am. Chem. Soc.* **127** 15536
[44] Gautier C and Bürgi T 2006 *J. Am. Chem. Soc.* **128** 11079
[45] Gautier C, Taras R, Gladiali S and Buergi T 2008 *Chirality* **20** 486
[46] Zhu M Z, Aikens C M, Hendrich M P, Gupta R, Qian H F, Schatz G C and Jin R 2009 *J. Am. Chem. Soc.* **131** 2490
[47] Cao G J, Schwarz W H and Li J 2015 *Inorg. Chem.* **54** 3695
[48] Gao Y, Dai X, Kang S G, Jimenez-Cruz C A, Xin M, Meng Y, Han J, Wang Z and Zhou R 2014 *Sci. Rep.* **4** 5862
[49] Yadav B D and Kumar V 2010 *Appl. Phys. Lett.* **97** 133701
[50] Mariscal M M, Oviedo O A and Leiva E P M 2012 *Metal Clusters and Nanoalloys: From Modeling to Applications* (Now York: Springer Science & Business Media)
[51] Kaltsoyannis N 2003 *Chem. Soc. Rev.* **32** 9
[52] Wang D, van Gunsteren W F and Chai Z 2012 *Chem. Soc. Rev.* **41** 5836
[53] Hayton T W 2013 *Chem. Commun.* **49** 2956
[54] Pyykkö P 1988 *Chem. Rev.* **88** 563
[55] van Lenthe E, Ehlers A and Baerends E J 1999 *J. Chem. Phys.* **110** 8943
[56] van Lenthe E, Baerends E J and Snijders J G 1993 *J. Chem. Phys.* **99** 4597
[57] van Lenthe E, Snijders J G and Baerends E J 1996 *J. Chem. Phys.* **105** 6505
[58] van Lenthe E, Baerends E J and Snijders J G 1994 *J. Chem. Phys.* **101** 9783
[59] van Lenthe E and Baerends E J 2003 *J. Comput. Chem.* **24** 1142
[60] Kutepov A 2007 *J. Alloys Compd.* **444** 174
[61] Ingram K I, Tassell M J, Gaunt A J and Kaltsoyannis N 2008 *Inorg. Chem.* **47** 7824
[62] Wåhlin P, Danilo C, Vallet V, Réal F, Flament J P and Wahlgren U 2008 *J. Chem. Theor. Comput.* **4** 569
[63] Cao X and Dolg M 2004 *J. Mol. Struc.* **673** 203
[64] Jiang D E, Kühn M, Tang Q and Weigend F 2014 *J. Phys. Chem. Lett.* **5** 3286
[65] Aikens C M 2011 *J. Phys. Chem. Lett.* **2** 99
[66] Iwasa T, Nobusada K and Nakajima A 2013 *J. Phys. Chem. C* **117** 24586
[67] Rauhalahti M and Mu?noz-Castro A 2015 *RSC Adv.* **5** 18782
[68] Neugebauer J, Reiher M, Kind C and Hess B A 2002 *J. Comput. Chem.* **23** 895
[69] Zhao L, Jensen L and Schalz G C 2006 *J. Am. Chem. Soc.* **128** 2911
[70] Neukermans S, Janssens E, Tanaka H, Silverans R E and Lievens P 2003 *Phys. Rev. Lett.* **90** 033401
[71] Zhai H J, Li J and Wang L S 2004 *J. Chem. Phys.* **121** 8369
[72] Gong X G and Kumar V 1993 *Phys. Rev. Lett.* **70** 2081
[73] Li X, Kiran B, Cui L F and Wang L S 2005 *Phys. Rev. Lett.* **95** 253401
[74] Gagliardi L 2003 *J. Am. Chem. Soc.* **125** 7504
[75] Roos B O, Malmqvist P Å and Gagliardi L 2006 *J. Am. Chem. Soc.* **128** 17000
[76] Halcrow M A 2013 *Chem. Soc. Rev.* **42** 1784
[77] Sato T, Lijnen E and Ceulemans A 2014 *J. Chem. Theor. Comput.* **10** 613
[78] Pyykkö P and Atsumi M 2009 *Chem. Eur. J.* **15** 186
[79] Janssens E, Tanaka H, Neukermans S, Silverans R E and Lievens P 2003 *New J. Phys.* **5** 46
[80] Li X, Kiran B, Cui L F and Wang L S 2005 *Phys. Rev. Lett.* **95** 253401
[81] Holtzl T, Janssens E, Veldeman N, Veszpremi T, Lievens P and Nguyen M T 2008 *Chem. Phys. Chem.* **9** 833
[82] Häkkinen H and Landman U 2000 *Phys. Rev. B* **62** R2287
[83] Zhao L X, Feng X J, Zhang M and Luo Y H 2010 *J. Clust. Sci.* **21** 701
[84] Negishi Y, Nobusada K and Tsukuda T 2005 *J. Am. Chem. Soc.* **127** 5261
[85] Lopez-Acevedo O, Tsunoyama H, Tsukuda T and Aikens C M 2010 *J. Am. Chem. Soc.* **132** 8210
[86] Wu D Y, Hayashi M, Chang C H, Liang K K and Lin S H 2003 *J. Chem. Phys.* **118** 4073
[87] Wu D Y, Hayashi M, Lin S H and Tian Z Q 2004 *Spectrochim Acta Part A* **60** 137
[88] Jensen L, Zhao L L and Schatz G C 2007 *J. Phys. Chem. C* **111** 4756
[89] Tian Z Q, Ren B and Wu D Y 2002 *J. Phys. Chem. B* **106** 9463
[90] Wu D Y, Liu X M, Duan S, Xu X, Bin B, Lin S H and Tian Z Q 2008 *J. Phys. Chem. C* **112** 4195
[91] Aikens C M and Schatz G C 2006 *J. Phys. Chem. A* **110** 13317
[92] Shinohara H 2000 *Rep. Prog. Phys.* **63** 843
[93] Dai X, Gao Y, Jiang W, Lei Y and Wang Z 2015 *Phys. Chem. Chem. Phys.* **17** 23308
[94] Jiang W and Wang Z 2015 *J. Cluster Sci.* **27** 845
[95] Alivisatos A P 1996 *Science* **271** 933
[96] Wu Z N, Liu J L, Gao Y, Liu H W, Li T T, Zou H Y, Wang Z G, Zhang K, Wang Y, Zhang H, *et al.* 2015 *J. Am. Chem. Soc.* **137** 12906
[97] Gao Y, Zhou B, Kang S G, Xin M, Yang P, Dai X, Wang Z and Zhou R 2014 *RSC Adv.* **4** 27146
[98] Gill R, Zayats M and Willner I 2008 *Angew. Chem. Int. Ed.* **47** 7602
[99] Smith A M and Nie S 2008 *J. Am. Chem. Soc.* **130** 11278
[100] Kilina S, Ivanov S and Tretiak S 2009 *J. Am. Chem. Soc.* **131** 7717
[101] Pradhan M, Sarkar S, Sinha A K, Basu M and Pal T 2011 *Crysteng-comm* **13** 2878